New Journal of Physics
The open access journal at the forefront of physics

Deutsche Physikalische Gesellschaft DPG
IOP Institute of Physics

Published in partnership with: Deutsche Physikalische Gesellschaft and the Institute of Physics

OPEN ACCESS

RECEIVED
6 October 2021

REVISED
17 March 2022

ACCEPTED FOR PUBLICATION
31 March 2022

PUBLISHED
6 May 2022

PAPER

Enforcing Levy relaxation for multi-mode fibers with correlated disorder

Yaxin Li[1], **Doron Cohen**[2] **and Tsampikos Kottos**[1,*]

[1] Wave Transport in Complex Systems Lab, Physics Department, Wesleyan University, Middletown CT-06459, United States of America
[2] Department of Physics, Ben-Gurion University of the Negev, Beer-Sheva 84105, Israel
[*] Author to whom any correspondence should be addressed.

E-mail: tkottos@wesleyan.edu

Keywords: generalized Levy dynamics, multimode systems, random matrix theory

Abstract

Environmental perturbations and noise are source of mode mixing and interferences between the propagating modes of a complex multi-mode fiber (MMF). Typically, they are characterized by their correlation (paraxial) length, and their spectral content which describes the degree of coupling between various modes. We show that an appropriate control of these quantities allows to engineer Levy-type relaxation processes of an initial mode excitation. Our theory, based on random matrix theory modeling, is tested against realistic simulations with MMFs.

1. Introduction

Multi-mode wave dynamics in the presence of noisy environmental perturbations has always been a topic of interest for a variety of frameworks ranging from quantum and matter waves to classical waves. In typical circumstances, noise is considered an evil, since it degrades the efficiency of the structures employed to perform useful operations on these waves. For example, in the frame of quantum electronics, optics and matter wave physics noise is responsible for decoherence effects, being damaging to emerging quantum information and computation technologies [1–4]. In a similar manner, in classical wave technologies (e.g. optics, microwaves or acoustics), noise pollutes the signal carried by a propagating wave, thus degrading the transfer of information [5–7]. It is perhaps for this particular reason that researchers have explored, over the years, various strategies to eliminate noise sources. An alternative approach would be to utilize its presence, and via appropriate design use it in order to control the signal propagation.

An example where such strategy might be useful, comes from the area of fiber communication and data processing, where single-mode fibers have reached their limitation as far as information capacity is concerned [8, 9]. Instead, multi-mode fibers (MMFs) and/or multi-core fibers (MCF) offer new exciting opportunities since their modes can be used as extra degrees of freedom for carrying additional information—thus increasing further the information capacity [9, 10]. Unfortunately, MMF suffer from mode coupling due to environmental perturbations (index fluctuations, fiber bending etc), occurring along the paraxial direction of propagation which both cause crosstalk and interference between propagating signals in different modes [10–17]. Under such conditions, one typically expects fast relaxation of an initial mode excitation in the mode-space and thus degradation of the information carried by the signal.

In this arena, several studies [18–23] have highlighted the success of random matrix theory (RMT) modeling which, within the framework of multiple input multiple output (MIMO) signal processing techniques, provide a satisfactory description of modal cross-talking. Originally developed for the description of wireless communications, the MIMO approach can be also adopted to MMF/MCF optics settings by associating the multiple channels to the multiple modes and/or multiple cores in the fiber. In this framework, the transmission channels were modeled as a random complex unitary matrix [18–20], thus allowing for an analytical treatment of the statistical properties of the so-called MIMO mutual information which provides the fundamental performance measure of the channel capacity.

2. Outline

Below we develop a protocol that controls the relaxation process of an initial mode excitation towards its ergodic limit $\sim 1/N$, where N is the dimensionality of the mode space. The mode mixing is due to quenched disorder associated with external perturbations along the propagation direction z of a MMF. The proposed scheme is based on the manipulation of these dynamical perturbations that are responsible for the mixing between the various modes. They are characterized by a spectral exponent $s \in [-1, 1]$ and by a correlation length z_c. We show that the relaxation process is given by a generalized Levy-law with a power exponent $\alpha \in [0, 2]$ that is dictated by the spectral content of the deformation. The generic prediction is based on RMT modelling [13, 18–23], and then tested against simulations with a MMF. In the latter context we provide a simple recipe for engineering the spectral content of the external perturbations, by designing the roughness of the fiber cross-section. Although our analysis refers to MMFs, the proposed methodology will have ramifications in other fields, ranging from decoherence management in quantum dots, matter waves and quantum biology [24–29], to acoustics and control of mechanical vibrations [5–7].

3. Modeling

We assume that imperfections induce coupling only between forward propagating modes (paraxial approximation). Furthermore, these perturbations vary with the propagation distance z. The z-dependent Hamiltonian H that describes the field propagation along the MMF can be written as $H = H_0 + V(z)$ where H_0 describes the unperturbed fiber, and $V(z)$ is a spatial-dependent potential characterized by a correlation function $\langle V(z')V(z'')\rangle = \mathcal{C}[(z' - z'')/z_c]$. We assume that the correlation function does not have heavy tails, and therefore, in practice, the fiber can be regarded as a chain of L uncorrelated segments, indexed by $t = 1 \ldots L$. The paraxial Hamiltonian that describes the field propagation within the t segment is $H^{(t)} = H_0 + \varepsilon B^{(t)}$, where ε indicates the strength of the perturbation. In the mode-basis of the unperturbed system, the $N \times N$ matrix H_0 is diagonal, with elements $(H_0)_{nm} = \delta_{nm}\beta_n$, where $\beta_1 < \beta_2 < \ldots \beta_N$ are the propagation constants of the modes $n = 1, 2, \ldots, N$. In this basis, the constant perturbation matrix $B^{(t)} = \left(B^{(t)}\right)^{\dagger}$ is responsible for the mode mixing. We assume that the perturbations associated with each concatenated segment are uncorrelated with one-another, namely, for $t \neq t'$ the correlation $\langle B^{(t)}_{n,m} B^{(t')}_{n',m'}\rangle$ is zero. The statistical dependence of $\langle |B_{n,m}|^2\rangle$ on $|n - m|$, aka lineshape of the band profile, reflects the spectral content of the perturbations. Specifically we consider below an *engineered* bandprofile that is characterized by power-law tails

$$|B_{n,m}|^2 \sim \frac{2}{|n-m|^s}, \quad \text{where} \quad -1 < s < 1. \tag{1}$$

The field propagation in each section is described by the unitary matrix

$$U^{(t)} = \mathrm{e}^{-\mathrm{i}(H_0 + \varepsilon B^{(t)})z_c}. \tag{2}$$

The modal field amplitudes $\Psi_n(z) \equiv \langle n|\Psi^{(t)}\rangle$ at distance $z = t \times z_c$ along the MMF are obtained by operating on the initial state $\Psi_n(0) = \delta_{n,n_0}$ with a sequence of $U^{(t)}$ matrices. This multi-step dynamics generates a distribution $P_z(n|n_0) = |\Psi_n(z)|^2$.

RMT considerations (that we outline below) imply that for large correlation length, the relaxation process is formally like a Levy-flight, for which the survival probability exhibits a power-law decay

$$\mathcal{P}(z) \equiv \overline{P_z(n_0|n_0)} \sim \left(\frac{1}{z}\right)^{1/\alpha}; \quad \text{where } \alpha = 1 + s. \tag{3}$$

The overbar indicates an average over different disorder realizations and initial conditions n_0. The different initial conditions were taken within a small energy window $n_0 \in [N/2 - N/100, N/2 + N/100]$ in order to ensure that the chosen initial preparations have the same statistical properties. In all our simulations the system size was taken to be $N > 500$. The evolving profile was then re-centered at $n_0 = N/2$ and processed for averaging. In all cases, we have average more than 100 different realizations of the generated dynamics. Note that $\alpha = 1$ is equivalent to the traditional RMT case, where B can be regarded as a random matrix realization of a Gaussian ensemble, otherwise we are dealing here with a so-called *banded* random matrix. However, we allow negative values of s, for which the size of the off-diagonal elements grows up as a function of $|n - m|$. We impose $s > -1$ for the following reason: as explained later $\alpha \leqslant 0$ implies a spreading kernel that has infinite norm and the model becomes formally ill-defined. An RMT demonstration of this decay is provided in figure 1, and further discussed later. In the RMT simulations the

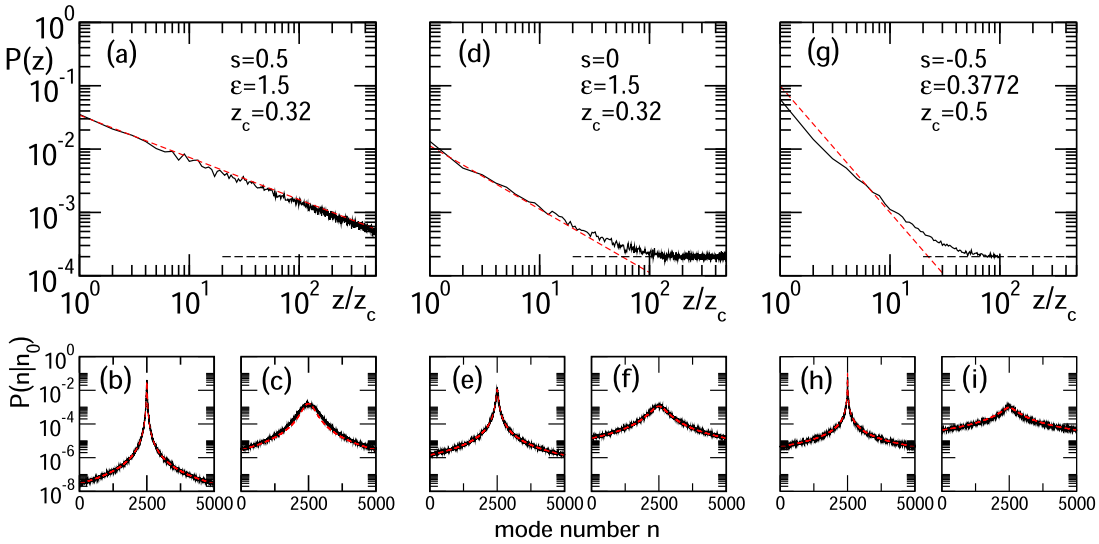

Figure 1. We consider here an RMT-modelled propagation of a pulse in a MMF with $N = 5000$ modes. Namely, $B_{n,m}$ is a random banded matrix, with a band profile given by equation (1), and the β_n are equally spaced. The results are averaged over more than 50 disorder realizations. The upper row shows the decay of the survival probability for bandprofile with (a) $s = 0.5$; (d) $s = 0$; and (g) $s = -0.5$. The values of ϵ and z_c are indicated in the figures. The decay is described by a power-law (red line) with power exponents $\alpha = s + 1$, given by equation (17). The black dashed lines indicate the ergodic limit $1/N$. Panels (b), (e) and (h) the waveprofile after a propagation distance $z = z_c$. The red dashed lines represent the theoretical prediction equation (14). Panels (c), (f) and (i) the waveprofile for $z/z_c = 100, 10, 10$ respectively. In all cases, the black solid lines represent simulation data and the red dashed lines represent the theoretical predictions.

β_n are equally spaced. The units of time are chosen such that the spacing is $\Delta = 1$. The band profile (off-diagonal terms) are given by equation (1), where the units of ε are chosen such that the pre-factor equals unity.

4. Engineered bandprofile

We consider a cylindrical fiber with core radius a. We assume TM propagating waves in the fiber. The solutions of the Helmholtz equation, under the requirement that the eigenmodes are finite at $r \to 0$, take the form

$$\Psi^{\nu,\ell}(r,\theta,z) = C_{\nu,\ell} J_\nu \left(\frac{x_{\nu,\ell}}{a} r\right) \mathrm{e}^{\mathrm{i}\nu\theta}\, \mathrm{e}^{\mathrm{i}\beta_{\nu,\ell} z}, \tag{4}$$

where $\Psi(r,\theta,z)$ is the electric field of the TM mode, ν is the azimuthal mode index, ℓ is the radial mode index, $J_\nu(\cdot)$ is the first-type Bessel function of order ν and $C_{\nu,\ell}$ is a normalization constant. The argument $x_{\nu,\ell}$ indicates the zeroes of the Bessel functions and for simplicity we only considered right-hand polarization. In case of a metal -coated core, the electric field satisfies the boundary conditions $\Psi(a,\theta,z) = 0$ and $\frac{\partial}{\partial\theta}\Psi(a,\theta,z) = 0$. These lead to the following quantization for the propagation constants for forward propagating waves in the (ν,ℓ) channel

$$\beta_{\nu,\ell} = \sqrt{\left(\frac{\omega}{c}\right)^2 - \left(\frac{x_{\nu,\ell}}{a}\right)^2}, \tag{5}$$

where c is the speed of light in the fiber medium. In our simulations below, the core-index is $\bar{n} = 1.5$, and the incident light has $\lambda_{\mathrm{vac}} = 1.55\ \mu$m.

Next, we enforce a pre-designed mode-mixing between the modes of the cylindrical (perfect) fiber via engineered boundary deformations. It turns out that a boundary deformation $D(\theta)$ due to e.g. surface roughness of the fiber, is related to the perturbation matrix $B_{nn'}$ via a 'wall' formula [33, 34]

$$B_{n,n'} = \oint \partial\Psi_n(\theta)\partial\Psi^*_{n'}(\theta) D(\theta)\mathrm{d}\theta, \tag{6}$$

where the sub-index indicates $n \equiv (\nu,\ell)$. In equation (6) the integration is along the boundary, and ∂ indicates the normal derivative. Substitution of the eigenmodes of the unperturbed fiber equation (4) in equation (6) leads to the following expression for the matrix elements of the B-matrix

$$\langle \nu,\ell|B|\nu',\ell'\rangle = c_{\nu,\ell} c_{\nu',\ell'} b_{\nu,\nu'}, \tag{7}$$

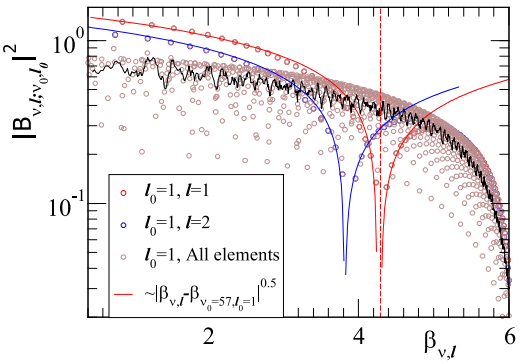

Figure 2. The matrix elements $|B_{\nu\ell,\nu_0\ell_0}|^2$ for an $N = 1031$ MMF with core radius $a = 15$ μm, calculated using equation (7) for $s = -0.5$. The red symbols are for the $\ell = \ell_0 = 1$ block. The other symbols are the couplings to the $\ell \neq \ell_0$ modes. The solid lines indicate the $\propto |\nu - \nu_0|^{-s}$ lineshape that is implied by equation (10). If all the ℓ modes are included (brown symbols) the averaged bandprofile (black line) features $s_{\rm eff} = 0$ lineshape.

where $c_{\nu,\ell} = C_{\nu,\ell} J_n'(\frac{x_{\nu,\ell}}{a} r)|_{r=a}$. The matrix elements within each ℓ-block are essentially the Fourier transform (FT) of the azimuthal deformation $D(\theta)$ i.e.

$$b_{\nu,\nu'} = \oint D(\theta) \mathrm{e}^{\mathrm{i}(\nu-\nu')\theta} \frac{\mathrm{d}\theta}{\pi}. \tag{8}$$

From equation (8) it is straightforward to identify the appropriate deformations $D(\theta)$ whose FT lead to perturbation matrices B with a desired power-law bandprofile, see equation (1). A simple recipe is to introduce $D(\theta)$ as a cosinus-Fourier series with coefficients that are random phases [35]. Namely,

$$D(\theta) = \sum_{q=1}^{N} \sqrt{Q_q}\, \cos(q\theta + \varphi_q) \tag{9}$$

with $Q_q = q^{-s}$, while φ_q is a random phase in the interval $[0, 2\pi)$. Substitution of the above deformation families back to equation (8) leads to the following band-profile for the ℓth block sub-matrix

$$|b_{\nu,\nu'}|^2 = |Q_{|\nu-\nu'|}| = \frac{1}{|\nu - \nu'|^s}. \tag{10}$$

The band profile that is implied by equation (7) with equation (10) is illustrated in figure 2 for an MMF with core radius $a = 15$ μm, and perturbation that features $s = -0.5$. The standard way to plot a band profile is a scatter plot of the squared elements $|\langle \nu, \ell|B|\nu_0, \ell_0\rangle|^2$ versus the off-diagonal coordinate $\omega = \beta_{\nu,\ell} - \beta_{\nu_0,\ell_0}$. In standard RMT models the β-s are equally spaced, and therefore ω is like the $n - m$ in equation (1). Here we have composite indexes, but nevertheless, in view of equation (5), there is a monotonic relation between β and ν. Therefore, if we keep a single ℓ block (say $\ell_0 = 1$) the band profile features power-law tails as a function of $\nu - \nu_0$, which is implied by equation (10). But if we include all the ℓ modes, we get an averaged bandprofile that is not singular at $\beta_{\nu,\ell} \sim \beta_{\nu_0,\ell_0}$, meaning an effective exponent $s_{\rm eff} = 0$.

5. RMT framework

The disordered nature of the perturbations allows RMT modeling for the matrix $B^{(t)}$, see [10, 13, 15, 16, 18–23]. Within the RMT framework, the matrix elements are not calculated but generated artificially. Specifically, we assume that the elements are uncorrelated random numbers drawn from a normal distribution centered at zero. We further assume, *dogmatically*, that they have variance in accordance with the power law lineshape of equation (1), and that the mode propagation constants are equally spaced, namely, $\beta_n = n\Delta$, where $n = 1, \ldots, N$. We will use the RMT modeling as a benchmark against which we shall compare the results from MMF simulations that use *engineered* bandprofiles.

The present section provides the analysis that explains the anomalous decay that has been demonstrated, using simulations, for an artificial RMT model in figure 1, in agreement with the predicted power law of equation (3) (dashed red lines). The artificial RMT model involves a random banded matrix $B_{n,m}$ with a well-defined band profile, as opposed to the rather complex structure of $\langle \nu, \ell|B|\nu', \ell'\rangle$ of a realistic MMF. In

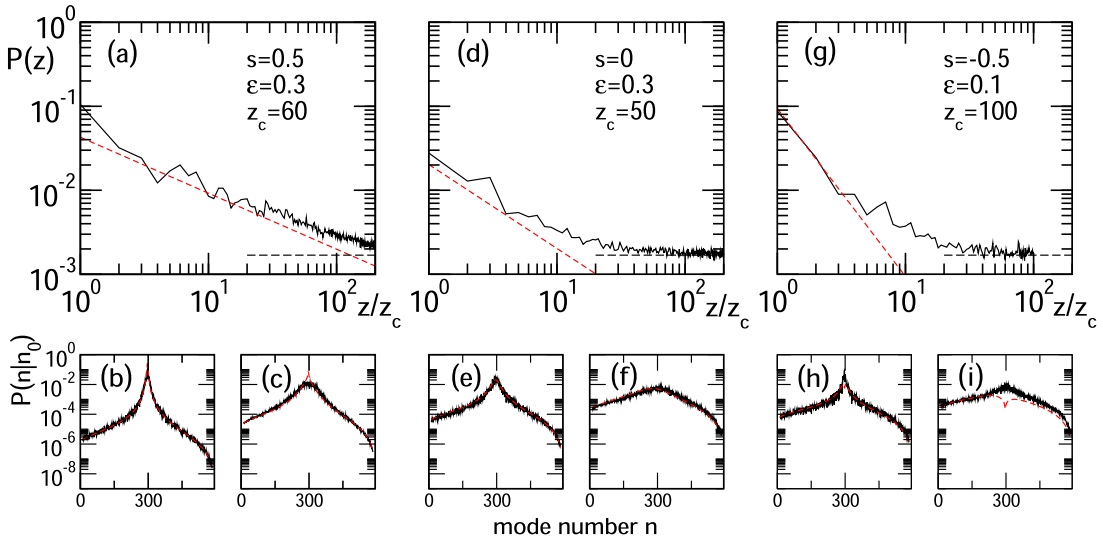

Figure 3. The MMF has core radius $a = 100\ \mu$m, and $N = 593$ modes. All the modes are confined within the $\ell = 1$ subgroup, and re-labeled by a running index n, such that the initial mode is $n_0 \sim N/2$. The results are averaged over ∼100 realizations of the rough surface. The results are averaged over initial conditions and realizations of the rough surface. The decay of the survival probability follows the power-law prediction equation (17) with (a) $s = 0.5$; (d) $s = 0$; and (g) $s = -0.5$ (red dashed lines). Panels (b), (e) and (h) the waveprofile after a propagation distance $z = z_c$. Panels (c), (f) and (i) the waveprofile for $z/z_c = 10, 5, 5$ respectively. The solid lines represent simulation data and the red dashed lines represent theoretical predictions.

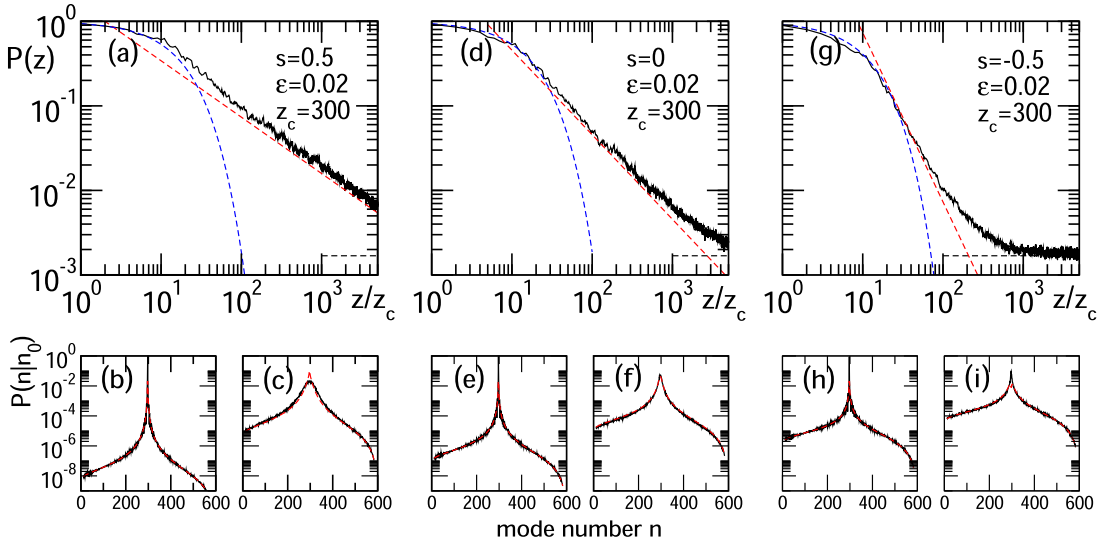

Figure 4. The same as in figure 3 for disorder that features $z_c < z_\Gamma$. Consequently an intermediate exponential stage appears (blue lines). Panels (b), (e) and (h) the waveprofile after a propagation distance $z = z_c$. Panels (c), (f) and (i) the waveprofile for $z/z_c = 1000, 100, 25$.

the subsequent sections we clarify whether such anomalous decay emerges in the latter case. The artificial RMT analysis provides a way to anticipate and to interpret the actual z dependence of the signal.

The correlation length z_c plays a major role in the decay of the survival probability. It has been argued [13] on the basis of analogy with Fermi-golden-rule that the strength ε of the perturbation translates into a length scale $z_\Gamma = (\varepsilon^2/\Delta)^{-1}$. If we have $z_c < z_\Gamma$ there is an intermediate stage during which the decay is exponential $\mathcal{P}(z) \propto \mathrm{e}^{-\lambda z}$, see details in [13]. Otherwise the decay is power law (see details below). Stand alone power-law decay for $z > z_c > z_\Gamma$ is demonstrated in figure 1 for representative values of s.

Following an argument that extends first-order perturbation theory [13, 30–32] the spreading kernel will saturate, for long enough z_c, to a generalized-Lorentzian line shape $\mathrm{Prob}(n|n_0) = W(n - n_0)$ that is characterized by a power law tail, namely,

$$W(n-n_0) \sim \frac{\varepsilon^2 |B_{n,n_0}|^2}{[(n-n_0)\Delta]^2} \sim \frac{(\varepsilon/\Delta)^2}{|n-n_0|^{1+\alpha}}, \tag{11}$$

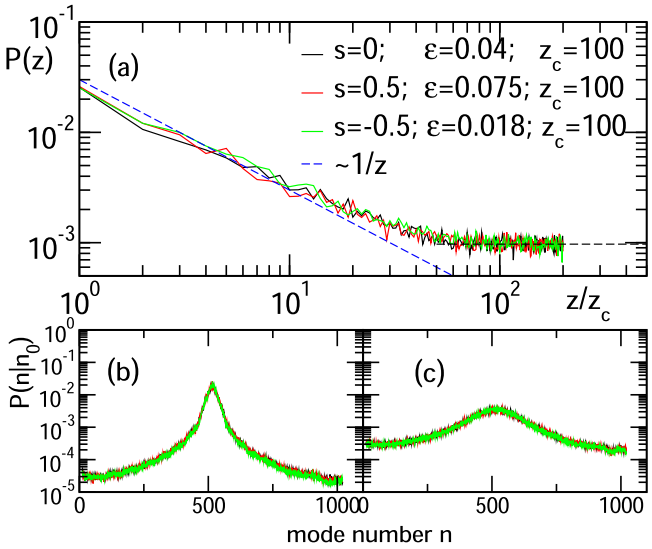

Figure 5. The $N = 1031$ modes for different ℓ-groups are mixed together via the perturbation matrix B. A ballistic decay with $\alpha = 1$ (blue dashed line) is observed irrespective of the s-value. The core radious is $a = 15$ μm.

where $\alpha = 1 + s$. In order to calculate the spreading profile after a propagation distance z, one has to perform $t = z/z_c$ successive convolutions. If the kernel has finite second-moment, which is the case for $\alpha > 2$, one obtains Gaussian spreading, as implied by the central limit theorem. This would lead to $P(z) \propto \sqrt{1/z}$ decay of the survival probability. Our interest below is in $0 < \alpha < 2$, which leads to an anomalous so-called Levy-process.

For the purpose of successive convolutions, the $W(r)$ kernel can be approximated as the FT of $w(\kappa) = \exp(-|\gamma\kappa|^\alpha)$, where γ is a fitting constant. Generally, these type of distributions do not have analytic expressions. However, assuming that the kernel obeys one-parameter scaling, it follows from normalization that

$$\gamma = C\Big(\frac{\varepsilon}{\Delta}\Big)^{2/\alpha}, \tag{12}$$

where C is a numerical prefactor of order unity. Successive convolutions lead to the Levy α-stable distribution. Namely, after t steps $\mathrm{Prob}_t(n|n_0)$ will be the FT of $[w(\kappa)]^t$. This means that the width parameter evolves as $\gamma \mapsto \gamma t^{1/\alpha}$. The survival probability is simply the area of $\exp(-t|\gamma\kappa|^\alpha)$, and accordingly we get

$$\mathcal{P}(z) = \frac{1}{\gamma}\Big(\frac{z_c}{z}\Big)^{1/\alpha}. \tag{13}$$

Note the special cases $\alpha = 1, 2$ that correspond to Lorentzian spreading and normal diffusion respectively. This result was our starting point equation (3), where it has been illustrated in figure 1. The practical determination of the pre-factor γ is further clarified in the following subsection.

5.1. Generalized Lorentzian

In practice we have to handle in our formulas the whole bandprofile. In the standard case $\alpha = 1$, and it is common to fit equation (11) into a Lorentzian. In general $\alpha \neq 1$, and we use for fitting a generalized Lorentzian (GL), namely,

$$W(n - n_0) \approx \frac{1}{\pi}\frac{\gamma^\alpha}{|n - n_0|^{1+\alpha} + \gamma^{1+\alpha}} \tag{14}$$

$$\mapsto \frac{2\varepsilon^2|B_{n,n_0}|^2}{|\beta_n - \beta_{n_0}|^2 + \Delta^{1-\alpha}\Gamma_{\mathrm{GL}}^{1+\alpha}}, \tag{15}$$

where in the second line we have manipulated the second term in the denominator: this term acts as a regularization parameter for the $n \sim n_0$ singularity, while at the tails it is negligible; therefore, for numerical purpose, only its near-diagonal value is important. For a smooth bandprofile the regularization parameter is

$$\Gamma_{\mathrm{GL}} = \gamma\Delta = \left(\frac{2\pi\varepsilon^2}{\Delta^{2-\alpha}}\right)^{1/\alpha} \tag{16}$$

and

$$\mathcal{P}(z) = \frac{1}{\pi}\frac{\Delta}{\Gamma_{\rm GL}}\left(\frac{z_{\rm c}}{z}\right)^{1/\alpha}; \quad \alpha = 1+s. \tag{17}$$

The convention we use for $\Gamma_{\rm GL}$ is such that for $\alpha = 1$ the Lorentzian (ballistic-like) decay of [13] is recovered. For a general bandprofile we determine $\Gamma_{\rm GL}$ via normalization of equation (15). We demonstrate in all our figures that this practical numerical procedure is a valid approximation.

6. Levy relaxation for a graded-index MMF

Coming back to the MMF, we have to realize that the band profile of equation (1) is not a valid model for the description of the actual matrix $\langle \nu, \ell | B | \nu', \ell' \rangle$. In order to design an MMF that features the desired power law decay of equation (3), we have to effectively eliminate transitions to $\ell \neq \ell_0$ modes, where ℓ_0 indicates the initial radial excitation. The latter constraint is achieved in case of graded-index MMFs [36]. The grading of the refraction index is like a radial potential. Such potential does not affect the form of equation (7), but it does shift 'horizontally' the branches of equation (5) that are illustrated in figure 2. Thus, effectively, only modes that belong to the same radial mode-group ($\ell = \ell_0$) are mixed, with perturbation matrix that is proportional to $b_{\nu,\nu'}$ of equation (10).

In our computational example we chose to focus on a low-ℓ radial group (e.g. $\ell = 1$) in order to minimize the effects of radiative losses. In figure 3 we have considered three representative values of s. Power law decay is demonstrated for a disordered MMF that has a correlation scale $z_{\rm c} > z_\Gamma$. The survival probability follows a Levy-type relaxation given by equation (17) with powers $\alpha = 1 + s$. Moreover, the probability distribution can be approximated by the GL of equation (15).

For completeness we have performed simulations for a MMF with disorder that has a correlation length $z_{\rm c} < z_\Gamma$, see figure 4. As expected form the analysis in [13], an intermediate exponential stage appears. This exponential decay reflects Fermi's golden rule. However, the long time decay becomes power law, as in figure 3, until the waveform reaches an ergodic distribution.

7. Universal relaxation

Having established that an RMT-like power law decay can be engineered for graded-index MMFs, we turn to consider an ungraded-index MMF. Transitions between modes that correspond to different ℓ-groups cannot be neglected, and therefore the bandprofile of the perturbation matrix B becomes effectively flat, see figure 2, irrespective of the spectral content of the deformation $D(\theta)$. Namely, the information about s is washed out once the propagation constants are ordered by magnitude and the ν indices are shuffled. Consequently, the survival probability $\mathcal{P}(z)$ for large correlation lengths (and large propagation distances) decays with $\alpha_{\rm eff} = 1$ irrespective of the value of s. The numerical demonstration is displayed in figure 5.

8. Summary

The interplay between the short time coherent evolution and the long time stochastic spreading in multimode systems is an intriguing theme. In this paper, we have demonstrated exponential and power law decay for pulse propagation in MMF. The latter is due to a Levy-type spreading. Specifically we find that general α Levy decay can be engineered for graded-index ring-core MMF, while universal $\alpha_{\rm eff} = 1$ is observed for MMFs with ungraded-index.

Our results have been benchmarked using an RMT perspective. The RMT toolbox facilitates studies whose aim is to design coupling schemes for which the coherent evolution leads to tailored anomalous decay of the signal. Specifically, the results of MMF simulations are benchmarked using an RMT perspective that involves banded random matrices.

It will be interesting to extend this line of study to cases where mode-dependent losses are also taken into consideration. We expect that the non-Hermitian nature of the dynamics, will lead to unexpected new phenomena. Another research direction is related to the effects of non-linearities in the mode-mixing. These questions are currently under investigation.

Acknowledgments

(YL) and (TK) acknowledge partial support by Grant No. 733698 from Simons Collaborations in MPS, and by an NSF Grant EFMA-1641109. (DC) acknowledges support by the Israel Science Foundation (Grant No. 283/18).

Data availability statement

The data that support the findings of this study are available upon reasonable request from the authors.

ORCID iDs

Yaxin Li https://orcid.org/0000-0001-8734-0136
Doron Cohen https://orcid.org/0000-0002-3835-3544

References

[1] Southwell K 2008 Quantum coherence *Nature* **453** 1003(and articles therein)
[2] Dowling J P and Milburn G J 2003 Quantum technology: the second quantum revolution *Phil. Trans. R. Soc.* A **361** 1655
[3] Andersson E and Öhberg P 2014 *Quantum Information and Coherence* (Berlin: Springer)
[4] Averin D V, Ruggiero B and Silvertrini P 2001 *Macroscopic Quantum Coherence and Quantum Computing* (Berlin: Springer)
[5] Brandt A 2011 *Noise and Vibration Analysis: Signal Analysis and Experimental Procedures* (New York: Wiley)
[6] Tuzlukov V I 2002 *Signal Processing Noise* (Boca Raton, FL: CRC Press)
[7] Norton M P and Karczub D G 2003 *Fundamentals of Noise and Vibration Analysis for Engineers* (Cambridge: Cambridge University Press)
[8] Keiser G 2000 *Optical Fiber Communications* 3rd edn (New York: McGraw-Hill)
[9] Kahn J M and Miller D A B 2017 Communications expands its space *Nat. Photon.* **11** 5
[10] Ho K-P and Kahn J M 2013 *Mode Coupling and its Impact on Spatially Multiplexed Systems, Optical Fiber Telecommunications VIB* (Amsterdam: Elsevier)
[11] Redding B, Alam M, Seifert M and Cao H 2014 High-resolution and broadband all-fiber spectrometers *Optica* **1** 175
[12] Xiong W, Ambichl P, Bromberg Y, Redding B, Rotter S and Cao H 2016 Spatiotemporal control of light transmission through a multimode fiber with strong mode mixing *Phys. Rev. Lett.* **117** 053901
[13] Li Y, Cohen D and Kottos T 2019 Coherent wave propagation in multimode systems with correlated noise *Phys. Rev. Lett.* **122** 153903
[14] Shemirani M B, Mao W, Panicker R A and Kahn J M 2009 Principal modes in graded-index multimode fiber in presence of spatial- and polarization-mode coupling *J. Lightwave Technol.* **27** 1248
[15] Ho K-P and Kahn J M 2011 Statistics of group delays in multimode fiber with strong mode coupling *J. Lightwave Technol.* **29** 3119
[16] Chiarawongse P, Li H, Xiong W, Hsu C W, Cao H and Kottos T 2018 Statistical description of transport in multimode fibers with mode-dependent loss *New J. Phys.* **20** 113028
[17] Wen X, Hsu C W, Bromberg Y, Antonio-Lopez J E, Correa R A and Cao H 2018 Complete polarization control in multimode fibers with polarization and mode coupling *Light: Sci. Appl.* **7** 54
[18] Winzer P J and Foschini G J 2011 MIMO Capacities and outage probabilities in spatially multiplexed optical transport systems *Opt. Express* **19** 16680
[19] Dar R, Feder M and Shtaif M 2013 The Jacobi MIMO channel *IEEE Trans. Inf. Theory* **59** 2426
[20] Karadimitrakis A, Moustakas A L and Vivo P 2014 Outage capacity for the optical MIMO channel *IEEE Trans. Inf. Theory* **60** 4370
[21] Nafkha A and Bonnefoi R 2017 Upper and lower bounds for the ergodic capacity of MIMO Jacobi fading channels *Opt. Express* **25** 12144
[22] Wei L, Liu C-H, Liang Y-C and Bai Z 2019 Matrix integral approach to MIMO mutual information statistics in high-SNR regime *Entropy* **21** 1071
[23] Laha A and Kumar S 2021 Optical MIMO communication with unequal power allocation to channels *Optik* **244** 167533
[24] Engel G S, Calhoun T R, Read E L, Ahn T-K, Mančal T, Cheng Y-C, Blankenship R E and Fleming G R 2007 Evidence for wavelike energy transfer through quantum coherence in photosynthetic systems *Nature* **446** 782
[25] Panitchayangkoon G, Hayes D, Fransted K A, Caram J R, Harel E, Wen J, Blankenship R E and Engel G S 2010 Long-lived quantum coherence in photosynthetic complexes at physiological temperature *Proc. Natl Acad. Sci. USA* **107** 12766
[26] Sarovar M, Ishizaki A, Fleming G R and Whaley K B 2010 Quantum entanglement in photosynthetic light-harvesting complexes *Nat. Phys.* **6** 462
[27] Lloyd S 2011 Quantum coherence in biological systems *J. Phys.: Conf. Ser.* **302** 012037
[28] Engel G S 2011 Quantum coherence in photosynthesis *Procedia Chem.* **3** 222
[29] Fleming G R, Scholes G D and Cheng Y-C 2011 Quantum effects in biology *Procedia Chem.* **3** 38
[30] Cohen D, Izrailev F M and Kottos T 2000 Wave packet dynamics in energy space, random matrix theory, and the quantum-classical correspondence *Phys. Rev. Lett.* **84** 2052–5
[31] Cohen D and Kottos T 2001 Parametric dependent Hamiltonians, wave functions, random matrix theory, and quantal-classical correspondence *Phys. Rev.* E **63** 036203
[32] Hiller M, Kottos T and Geisel T 2009 Wavepacket dynamics in energy space of a chaotic trimeric Bose–Hubbard system *Phys. Rev.* A **79** 023621
[33] Cohen D 2000 Chaos and energy spreading for time-dependent Hamiltonians, and the various regimes in the theory of quantum dissipation *Ann. Phys., NY* **283** 175
[34] Barnett A, Cohen D and Heller E J 2000 Deformations and dilations of chaotic billiards: dissipation rate, and quasi-orthogonality of the boundary wave functions *Phys. Rev. Lett.* **85** 1412
[35] Frahm K M and Shepelyansky D L 1997 Quantum localization in rough billiards *Phys. Rev. Lett.* **78** 1440
[36] Feng F *et al* 2017 All-optical mode-group multiplexed transmission over a graded-index ring-core fiber with single radial mode *Opt. Express* **25** 13773